Design of Hybrid Waveguide Structures for High-Efficiency Integrated Optical Superconducting Single Photon Detectors On Ti:$LiNbO_3$ Waveguides

Mikhail Parfenov, Petr Agruzov, Igor Ilichev, Sergey Bozhko, and Aleksandr Shamrai

***Abstract*—A configuration of integrated optical superconducting single photon detectors on lithium niobate substrates based on conventional titanium in-diffused waveguides with hybrid waveguide structures for enhancing the detector efficiency is proposed and analyzed. The sensing element in the form of a meander-like superconducting nanowire from niobium nitride is covered with an additional hybrid waveguide from a dielectric material with a higher refractive index than the $LiNbO_3$ substrate to increase the light absorption. A special mode converter in the region free from a superconducting nanostructure is used to excite a localized mode with the maximum absorption coefficient that strongly interacts with the superconductive nanostructure. Silicon and titanium dioxide are considered and compared as suitable materials for the hybrid waveguide structures. Silicon based structures give a higher light concentration and, hence, a higher absorption coefficient. However, they are very demanding to the technological accuracy. Titanium dioxide structures potentially can be produced by the standard thin-film deposition technique and contact photolithography. The estimated absorption coefficient of 1.31 dB/μm is four orders of magnitude higher than that for the detectors with a standard titanium in-diffused waveguide, and a high transformation mode efficiency opens a way for fabrication of integrated optical superconducting single photon detectors with the efficiency comparable with other competing material platforms.**

***Index Terms*—Integrated optics, optical waveguides, optoelectronic and photonic sensors, photonics, superconducting photodetectors.**

I. Introduction

LITHIUM niobate ($LiNbO_3$, LN) integrated optics has emerged over the last two decades as one of the key technological platforms for enabling monolithic integration of quantum photonic components and circuits on a chip [1]. Due to mature technological processes for waveguide fabrication [2] and also inherent optical effects for light control [3]–[10] and compatibility with the existing telecommunication infrastructures, $LiNbO_3$ integrated optical devices are nowadays at the heart of many quantum components (photon-pair or triplet sources, coherent wavelength convertors, quantum memories, optical modulators and linear optical quantum computing schemes) [1].

The development of scalable quantum computing architectures requires an on-chip integration of a variety of circuit elements, including single-photon detectors for analysis of photonic quantum states. In addition to the quantum application, highly efficient low-noise single-photon detectors are vital for the realization of numerous classical applications, such as optical time domain reflectometry and optical coherence tomography.

A superconducting single-photon detector (SSPD) [11] is a relatively simple architecture for the realization in an integrated optical configuration and has been demonstrated on several technological platforms [12]. It is based on the principle of photoinduced hot-spot formation in superconducting nanowires and can offer a high sensitivity at telecommunication wavelengths near 1550 nm, high counting rates, a broad spectral response, and a high temporal resolution due to a low jitter.

The SSPD on lithium niobate substrates was also considered [13]–[18]. A high quality and excellent superconducting properties of niobium nitride (NbN) nanofilms formed on $LiNbO_3$ substrates and, in particular, on titanium in-diffused waveguides (Ti:$LiNbO_3$) [19] were demonstrated. However, a low efficiency (lower than 1%) of integrated optical detectors based on Ti:$LiNbO_3$ waveguides was observed experimentally in spite of saturation of counts which indicated that the internal detection efficiency related to superconducting properties was maximized [20]. Thus, the main obstacle is an insignificant light absorption due to a rather large effective mode area of conventional Ti:$LiNbO_3$ waveguides and its small overlap (weak light interaction) with sensitive ultrathin NbN superconducting nanostructures. The technology of thin-film lithium-niobate-on-insulator (TFLNOI) waveguides has allowed an increase in the waveguide refractive index difference, squeeze effective mode area and an increase in the $LiNbO_3$ SSPD efficiency to the level comparable to rival integrated optical technologies [17].

In spite of many advantages of TFLNOI waveguides there are some technical problems. One of them is a complicated and very delicate pigtailing technique based on grating coupling or tapered lensed fibers [21] which is characterized by a rather high coupling loss and requires a precise alignment which should be stable at cryogenic temperatures. Another problem is the pyroelectric damage during cooling down to cryogenic

Manuscript received September 14, 2021; revised October 11, 2021; accepted October 14, 2021. Date of publication October 19, 2021; date of current version November 10, 2021. The work was supported by the Russian Science Foundation under Grant 19-19-00511. *(Corresponding author: Mikhail Parfenov.)*

Mikhail Parfenov is with the Ioffe Institute, St. Petersburg 194021, Russia and also with Peter the Great St. Petersburg Polytechnic University, St. Petersburg 195251, Russia (e-mail: mvparfenov@mail.ioffe.ru).

Petr Agruzov, Igor Ilichev, and Aleksandr Shamrai are with the Ioffe Institute, St. Petersburg 194021, Russia (e-mail: piotrag@mail.ioffe.ru; iiv@mail.ioffe.ru; achamrai@mail.ioffe.ru).

Sergey Bozhko is with the ISSP RAS, Chernogolovka, Moscow District 142432, Russia (e-mail: bozhko@issp.ac.ru).

Digital Object Identifier 10.1109/JPHOT.2021.3120930

temperatures [18] which is more considerable in the thin film configuration of TFLNOI waveguides. TFLNOI substrates also badly sustain high temperatures ($>$ 500 °C). This restricts the maximum temperature of technological processes which can be used for SSPD fabrication. In particular, a simple technology of reactive magnetron sputtering at a high temperature (800 °C) we used earlier for deposition of NbN film with the structure close to the epitaxial one [19] could not be used.

Besides the resistance to high temperatures the conventional Ti:$LiNbO_3$ waveguides have other advantages. Their fundamental mode can be matched to the standard single mode optical fiber [22]. Thus, the robust and simple endfire pigtailing [23] can be used. The SSPD nanostructure is patterned on a flat surface, which reduces a possible number of technological imperfections.

To make a step towards the development of SSPD on Ti:$LiNbO_3$ waveguides (LN-SSPD), we propose the approach involving an enhancement of a light interaction with sensitive superconducting nanostructures based on waveguide mode transformation in hybrid waveguide structures which cover NbN. The idea to use a cover layer for the LN-SSPD efficiency increase was considered earlier [24], however, a rigorous analysis and quantitative estimates were not given. The efficiency of optical photon interaction with a superconducting nanostructure can be described in terms of classical wave optics as absorption of optical waves propagating through a waveguide. The goals of this paper are to analyze theoretically a new integrated optical LN-SSPD, to estimate the efficiency of light absorption as a key quantitative characteristic of the SPPD efficiency and to choose the optimal design of LN-SSPD for a further experimental realization. The optimization criteria are a balance between a high absorption coefficient and high efficiency of an adiabatic waveguide mode transformation, and also the technical feasibility and a low sensitivity to technological imperfections.

II. Experimental Demonstration of SSPD on Titanium In-Diffused Lithium Niobate Waveguides

The simplest integrated optical SSPDs configuration is a straight waveguide covered with a superconducting nanostructure [12]. We fabricated the samples, which consisted of straight titanium in-diffused waveguides covered with a superconducting nanowire meander made of NbN. The titanium stripes with a thickness of 100 nm and width of 6 μm were used for the waveguide fabrication. The single-mode waveguides (in telecommunication wavelength range 1520-1580 nm) were formed after thermal diffusion at 1050 °C during 14 h. The waveguides had a high optical quality and their mode spot rather well matched the mode spot of the standard single mode optical fiber (SMF28). The measured fiber-to-fiber loss for endfire pigtailing of 50 mm samples was about 2.2 dB. Taking into account the intrinsic loss (about 0.02 dB/mm) which was measured by the low-finesse Fabry-Perot technique [25] the loss on the fiber-to-waveguide coupling was estimated to be 0.5 dB. This estimate was in agreement with the value calculated from the overlap integral of the waveguide and the optical fiber mode spots.

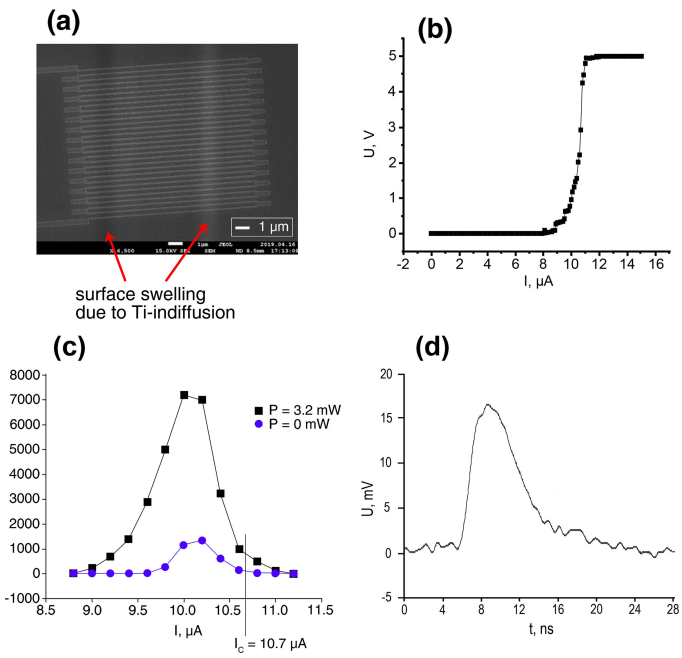

Fig. 1. Experimental demonstration of LN-SSPD: (a) SEM image of meander-like NbN nanostructure formed on a Ti:$LiNbO_3$ waveguide, (b) results of critical current measurements at 4.2 K, (c) measured photon counts versus bias current (squares) and dark counts (circles) (I_C – critical current), and (d) oscillogram of a single photon response.

NbN layers with a thickness of 5 nm were deposited on the waveguides by reactive magnetron sputtering of a Nb target in the Ar-N_2 atmosphere ($P_{Ar} = 4.5{\cdot}10^{-3}$ mBar, $P_{N2} = 8{\cdot}10^{-4}$ mBar) at a high temperature (800 °C). A DC plasma discharge with current I = 100 mA and voltage U = 500 V was used. The deposition rate was 0.1 nm/s. The root mean square (RMS) of NbN film surfaces measured by atomic force microscopy did not exceed 2Å. The NbN film deposition technology was described in detail in [19]. Moreover, it was shown that the superconducting properties of the films were not affected by the surface roughness [19]. Then the meander structures consisting of NbN nanowires with a width of 100 nm and period of 200 nm were produced on the area of 10 μm $\times$ 10 μm using electron-beam lithography (Fig. 1(a)). We used the nonoptimized structure typical of SSPD in our preliminary experiments. The measured critical current was about 10.7 μA at 4.2 K (Fig 1(b)). We used a rather high temperature of liquid helium at normal atmospheric pressure (4.2 K) which had a high stability and did not require a complicated technique for maintenance. It is very convenient for applications in spite of a possible decrease in the internal detection efficiency [26]. Experimental demonstration of single photon countings (Fig. 1(c)-(d)) showed a very low efficiency (much lower than 1%). The detection efficiency was measured with the help of a DFB laser diode at wavelength 1550 nm, a high extinction tunable optical attenuator, and a low noise electronic amplifier which was placed near the SSPD and immersed into liquid helium. The dependence of photon counts on the bias current is presented in Fig. 1(c). The absence of saturation in the dependence is the indication that the internal detection efficiency had not reached the maximum. We suppose that in addition to

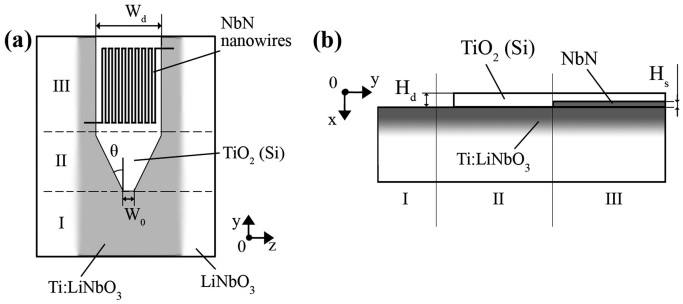

Fig. 2. Proposed integrated optical LN-SSPD design: (a) top view and (b) side view.

high temperature this was caused by the nonoptimized superconducting nanostructure configuration and could be corrected by directing nanowires along the optical waveguide and adjusting their width, height and the period of meander structure [20], [27]–[29].

The maximum internal detection efficiency should be accompanied by a high light absorption coefficient. We tried to measure the additional loss caused by the NbN nanostructures on the top of the Ti:$LiNbO_3$ waveguides at room temperature. It was very low and imperceptible against the background of variations in the fiber to waveguide loss (about ~ 0.1 dB) due to misalignment and end-face polishing defects. The waveguide structure had to be modified to increase the light absorption.

III. Design of Hybrid LN-SSPD

To increase light absorption by the superconducting nanostructure, a new design of the LN-SSPD based on a hybrid waveguides has been proposed. It consists of three sections (Fig. 2). The first input section I is a part of the substrate with a straight single-mode channel gradient Ti:$LiNbO_3$ waveguide. It performs the function of a light input from a standard single mode optical fiber. The light distribution at the end of Section I corresponds to the fundamental waveguide mode localized in $LiNbO_3$ and had a characteristic transverse size of about 10 μm [22].

Section III is the SSPD. The sensing element is a meander-like superconducting nanowire from NbN which is formed at the Ti:$LiNbO_3$ waveguide top. It is covered with an additional hybrid waveguide in the form of a stripe (W_d x H_d) of a dielectric material with a higher refractive index than the $LiNbO_3$ substrate. Silicon (Si) and titanium dioxide (TiO_2) are possible materials for the hybrid waveguide. These materials are transparent in the telecommunication wavelength range (1520–1580 nm) and are used as substrates for SSPD [12].

They do not make the NbN superconducting properties poorer. The technologies for fabrication of hybrid waveguides on $LiNbO_3$ substrates using these materials were experimentally demonstrated [30]–[32].

Section II is a hybrid waveguide mode transformer in the form of a taper with a smooth width increase at a constant height of the high-refractive-index cover stripe. An adiabatic transformation of the fundamental mode of the titanium in-diffused waveguide to the hybrid mode of Section III which is localized in the high-refractive-index stripe should occur in the taper.

IV. Numerical Simulation

The LN-SSPD on a $LiNbO_3$ substrate of the x-cut orientation with an optical waveguide directed along the y crystallographic axis was analyzed. This is the most common orientation for electrooptic modulators and other waveguide components on $LiNbO_3$ substrates [5] which efficiently operate with the quasi traverse hybrid waveguide modes polarized along the z axis (TE). As will be shown in the next section, the mode transformer without a polarization conversion can be designed to avoid a SSPD efficiency decrease due to polarization conversion.

The hybrid waveguide modes of the sensitive Section (III) were analyzed by two-dimensional finite-element method simulation (COMSOL) at telecommunication wavelength $\lambda = 1550$ nm. To reduce computational complexity, a simplified model of a titanium in-diffused waveguide was used. A gradient refractive index profile in the birefringent crystal substrate was represented as two step-index profiles: one for the extraordinary (TE) polarization and one for ordinary (TM) polarization. The widths, heights and refractive index contrasts of these step-index waveguides were determined by fitting theoretical modal field distributions to experimentally measured light intensity distribution in a typical single mode (at 1550 nm) titanium in-diffused waveguide [2], [22]. The single-mode titanium in-diffused waveguide had the parameters optimal for coupling with standard single-mode telecommunication fibers: the extraordinary refractive index of the $LiNbO_3$ substrate was $n_s{}^e = 2.140$, the effective waveguide refractive index was $n_w{}^e = 2.145$ and the effective gradient waveguide height and width were $H^{TE}{}_{LiNbO3} = 4.5$ μm and $W^{TE}{}_{LiNbO3} = 8.0$ μm, respectively, for the TE polarization. Note that the titanium in-diffused waveguide has other parameters ($n_s{}^o = 2.210$, $n_w{}^o = 2.212$, $H^{TM}{}_{LiNbO3} = 7.5$ μm and $W^{TM}{}_{LiNbO3} = 10.5$ μm) for the TM polarization because of the difference in the dependences of refractive index on titanium concentration for quasi TE and TM modes [22]. The sensitive superconducting nanostructure was in the form of a meander with the nanowires having width d and period D which were varied. The structure thickness was fixed $H_s = 5$ nm and corresponded to the film thickness in our preliminary experiments. The simulation was carried out for the NbN refractive index corresponding to its resistive state ($n_{NbN} = 5.23\text{-}5.28i$, [33]) since if the SSPD was operated at the bias currents near to the critical one the minimal interaction with light knocked the nanowire out of the superconducting state.

V. Maximization of Optical Absorption

The transverse dimensions (W_d and H_d) of the high-refractive-index stripe ($n_{TiO2} = 2.31$ [34] or $n_{Si} = 3.48$ [35]) were varied to find conditions for the maximum absorption coefficient. At first, we sought this condition for typical parameters of the superconducting nanostructure: nanowire width $d = 100$ nm and meander period $D = 200$ nm. Then the dimensions of the high-refractive-index stripe were fixed under the conditions of maximum absorption coefficient, and the superconducting

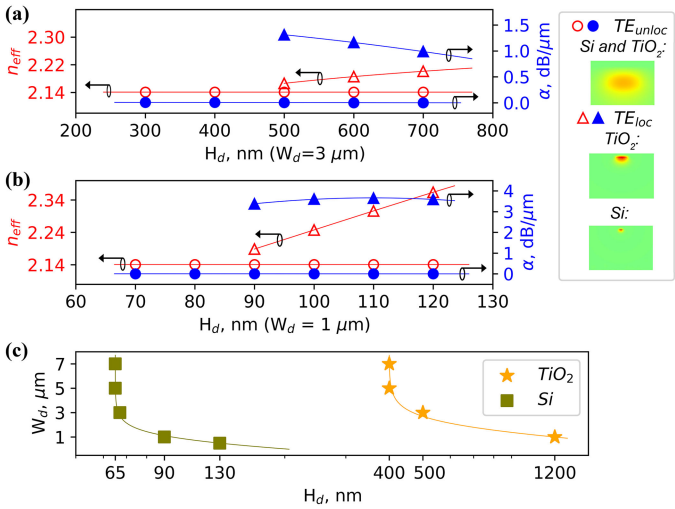

Fig. 3. Effective refractive indices and absorption coefficients of hybrid quasi TE modes versus high-refractive-index stripe heights H_d at fixed width W_d, superconducting nanowire width d = 100 nm and meander period D = 200 nm: (a) TiO_2 stripe (Wd = 3 μm), (b) Si stripe (W_d = 1 μm). The insets show the electric field profiles for the TE_{unloc} mode and TE_{loc} modes for the high refractive index stripes from TiO_2 and Si. (c) Cutoff conditions for TE_{loc} mode localized in the high-refractive-index stripe.

nanowire width d and meander period D were alternatively varied in order to reveal their influence on the absorption coefficient. The high-refractive-index stripe modified a spatial intensity distribution for the hybrid waveguide structure modes (see Fig. 3). A specific feature of the configuration was a rather weak interaction between the light in lithium niobate and in the high-refractive-index stripe. It is caused by the presence of the NbN superconducting nanostructure which separated these parts of the hybrid waveguide structure like a metal mirror. The conditions for a high absorption were the cutoff conditions of the hybrid quasi TE_{loc} mode which was localized in the high-refractive-index stripe, had a small effective mode area and was highly absorbed by the superconductor. The other mode (TE_{unloc}) was unlocalized and propagated mostly in lithium niobate. It had a weak interaction with the superconducting nanostructure. This is illustrated by the theoretical dependences of the effective refractive indexes and absorption coefficients of these two hybrid TE modes on the height (H_d) of the high-refractive-index stripe at a fixed stripe width W_d which are shown in Fig. 3. The cutoff conditions for the TE_{loc} mode could be fulfilled at different ratios between H_d and W_d (Fig. 3(c)). Note that the maximum absorption coefficient for this mode weakly depended on particular sizes of the high-refractive-index stripe. ${W_d}^{TiO2} = 3$ μm for TiO_2 stripe and ${W_d}^{Si} = 1$ μm we chose were rather low to give an appreciable light intensity concentration at the stripe height ${H_d}^{TiO2} = 500$ nm and ${H_d}^{Si} =$ 110 nm for TiO_2 and Si, respectively. The smaller mode effective area was for the Si stripe and, as a consequence, the absorption coefficient was also higher for the hybrid waveguide structure with the Si stripe than that with the TiO_2 stripe ($\alpha_{Si} = 3.65$ dB/μm and $\alpha_{TiO2} = 1.31$ dB/μm, respectively). However, TiO_2 is preferable from the technological point of view since larger sizes of the TiO_2 stripe are less demanding to the accuracy of fabrication. In addition, they are compatible with standard techniques of thin-film production and contact photolithography. The theoretical estimate of the achievable absorption coefficient is two times higher than that estimated for the thin-film lithium-niobate-on-insulator waveguide configuration [17] and four orders of magnitude higher than for the superconducting nanostructure on a standard Ti:$LiNbO_3$ waveguide. The theoretical estimate of the absorption coefficient shows that the length of sensitive Section III will be only 15.3 μm for achieving a 99% absorption for the TE_{loc} mode. Note that a shorter detector length is preferable because it provides a lower inductivity of the superconducting nanostructure and shorter SSPD response time. It should be also noted that the absorption rate was directly derived from the absorption coefficient, without consideration of other factors, such as efficiency of TE_{loc} mode excitation and reflection on the boundary between Section II and Section III. Their influence on detection efficiency will be considered further.

We have also analyzed the case when a superconducting nanostructure was placed over the high-refractive-index stripe. The conditions for maximum absorption were similar to the case when the superconducting structure was between a $LiNbO_3$ substrate and a high-refractive-index stripe, however, the maximum absorption coefficient was lower. The difference was very small for the Si stripe ($\alpha_{Si} = 1.98$ dB/μm) but for the TiO_2 stripe the absorption dropped dramatically ($\alpha_{TiO2} = 0.15$ dB/μm). As mentioned above, the absorption coefficient depends on the overlap between the superconducting structure and field of an optical mode. Due to different refractive index contrasts on the top and at the bottom of the dielectric stripe, the field of the TE_{loc} mode was shifted more to lithium niobate than to air. As a consequence, the absorption coefficient was lower when the superconducting nanostructure was placed over the stripe. This difference became significant as the refractive index of the dielectric stripe approached the refractive index of $LiNbO_3$. Thus, it was high for the TiO_2 stripe and imperceptible for the Si stripe.

Note that the conditions of the maximum light absorption were determined by transverse dimensions of the high-refractive-index stripe but did not depend on the superconducting nanostructure topology. The dependences of the maximum absorption coefficient on the nanowire width d and meander period D are shown in Fig. 4. The variation in the period and width of nanowires had a little effect on the absorption coefficient which slowly decreased as the filling of the superconducting layer became sparse**.** The subwavelength sizes of the superconducting nanostructure explain such behavior.

VI. Analysis of Mode Transformer

The light in the high-refractive-index dielectric stripe very weakly interacts with the light in $LiNbO_3$ in the SSPD configuration with a superconducting nanostructure between the titanium in-diffused waveguide and the high refractive index dielectric stripe. Thus, a mode transformer should be used. Very similar effective refractive indices of the fundamental TE_{LN} mode of

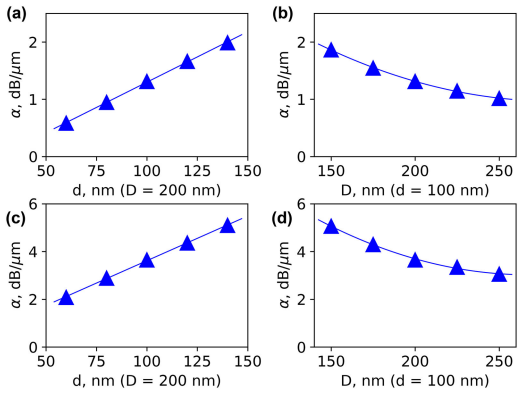

Fig. 4. Influence of the superconducting nanostructure topology (nanowire width d and meander period D) on the absorption coefficient for TiO_2 (a, b) and Si (c, d) stripes.

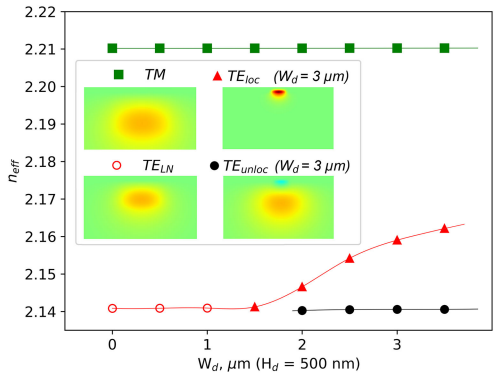

Fig. 5. Effective refractive index of waveguide modes versus TiO_2 taper width W_d at fixed height $H_d = 500$ nm. The insets show electric field profiles for different taper cross-sections.

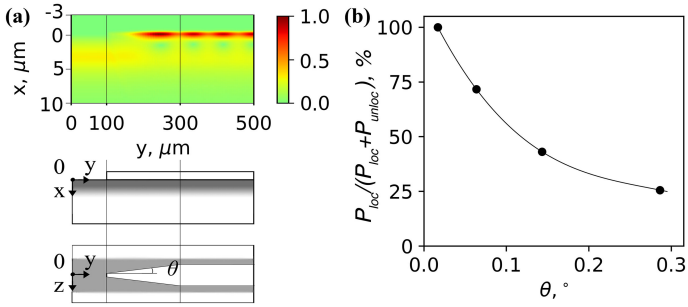

Fig. 6. Results of BPM simulation. (a) A typical picture of light propagation in the designed TiO_2 taper ($W_0 = 1$ μm, $\theta \approx 0.29°$, normalized intensity distribution). The fundamental TE_{LN} mode is launched to the mode transformer input. (b) Efficiency of mode transformation as a function of the half taper angle θ.

the titanium in-diffused waveguide in Section I and TE_{unloc} mode in sections II and III create a risk of light leakage to the TE_{unloc} mode and a decrease in the SSPD efficiency. Therefore, detailed analysis of light propagation in the mode transformer (Section II in Fig. 2) was carried out. The taper configuration for waveguide mode transformation should provide an adiabatic mode transformation. The TiO_2 taper will have larger sizes as compared to the Si taper, and adiabatic configuration can be easily realized by standard methods of thin-film technology and contact photolithography. Therefore, detailed analysis was carried out specifically for the TiO_2 taper.

The taper configuration (Fig. 2) was described by the following parameters: the taper height $H_d = 500$ nm and final width $W_d = 3$ μm were defined in the previous section from the conditions of a high light absorption. The initial width W_0 and half taper angle θ had to provide an adiabatic waveguide mode transformation. We set $W_0 = 1$ μm, which is a typical resolution of simple contact photolithography, and the influence of the taper angle was analyzed. Taper hybrid modes were analyzed by using the same two-dimensional finite-element method simulation (COMSOL) as the modes of sensitive Section III. Then the beam propagation method (BPM) was used to prove an adiabatic regime of operation and estimate the taper transformation efficiency. The fundamental mode of the gradient titanium in-diffused waveguide was used as an input signal.

The results of simulation are presented in Figs. 5 and 6. They show that the half taper angle should be much lower than the estimate for a simple titanium in-diffused taper $\theta < \frac{\lambda}{2W_{LiNbO3}n_W} \approx 4{\cdot}10^{-2}$ radian $\approx 2.3°$ [36]. The half taper angle θ less than $0.1°$ should ensure the mode transformation efficiency higher than 50%.

A limited efficiency of mode transformation lead to an excitation of the TE_{unloc} mode in sensitive Section III and to an interference between TE_{loc} mode and the TE_{unloc} mode. This explains the interference pattern obtained in the BPM simulation which was used for the estimation of the mode transformation efficiency (Fig. 6).

According to the simulation results, the effective refractive indices and mode field distributions of TE_{loc} modes on the taper output and in the Section III of the SSPD (at $W_d = 3$ μm and $H_d = 500$ nm) are slightly different. This difference is due to NbN nanostructure. The Fresnel reflection and leakage due to mode mismatch on the boundary between Section II and Section III were estimated as $3{\cdot}10^{-4}$% and 99.4%, respectively. Thus, this boundary has little effect on detection efficiency.

The theoretical analysis has also shown that the TM mode of the titanium in-diffused waveguide does not "feel" the taper and does not change the effective refractive index. In addition, the dispersion curves for the orthogonally polarized modes are far from each other and, as a consequence, there is no risk of polarization conversion [37]. It should also be noted that the untransformed TM mode has almost negligible propagation losses in Section III of LN-SSPD.

VII. Discussion

The theoretical analysis of an optimal LN-SSPD design showed that the evolutions of mode composition in taper Section II (Fig. 5) and in the detector region in Section III (Fig. 3) are different. The growth of the dielectric stripe height (H_d) and origin of the TE_{loc} mode do not distort the fundamental mode of the Ti:$LiNbO_3$ waveguide. At the same time, when the width (W) of a dielectric stripe in Section II without the NbN nanostructure (Fig. 5) increases, the fundamental mode of the Ti:$LiNbO_3$ waveguide can be converted to a TE_{loc} mode.

This difference can be explained by the influence of a NbN nanostructure which divides a hybrid waveguide into two parts like a metal mirror [38]. This behavior shows the main requirements to the LN-SSPD design. A mode with a high absorption can not be excited when the superconducting nanostructure is covered with an additional high-refractive-index dielectric layer. A special mode converter on the Ti:$LiNbO_3$ waveguide in the region free from a superconducting nanostructure should be used to excite a localized mode with the maximum absorption coefficient that, in turn, strongly interacts with the superconductive nanostructure. To prevent a light leakage, the converter should ensure an adiabatic mode transformation. We have analyzed the simplest design of such a converter which is a taper with a smooth width increase at a constant height of the high-refractive-index cover stripe. A very small taper angle ($< 0.1\ ^\circ$) is needed for the effective mode conversion even in the case of TiO_2 dielectric stripe with not very high refractive index increase relative to the Ti:$LiNbO_3$ waveguide. The requirement is more strict for the Si taper for which the refractive index increase is one order of magnitude higher. This makes the adiabatic Si taper fabrication challenging and demanding to the technology. This was our first argument for the choice of the TiO_2 stripe in spite of the fact that a higher absorption coefficient could be obtained with a Si stripe. Note that even the TiO_2 stripe increases the LN-SSPD absorption efficiency dramatically.

Note that the theoretical analysis was carried out and estimation of the LN-SSPD performance was made for an ideal hybrid waveguide structure with vertical and smooth sidewalls. While the verticality of the sidewalls had a little effect on the optimal LN-SSPD design, the scattering of optical waves from the sidewall roughness could lead to a significant degradation in the LN-SSPD efficiency. The technologies for fabrication of hybrid waveguides on $LiNbO_3$ substrates with rather a low optical loss were developed for the materials of interest (Si and TiO_2) [30]–[32], but TiO_2 which has a lower refractive index contrast has less strict requirements to fabrication imperfections [34], such as a deviation of the waveguide structure sizes and sidewalls roughness.

As mentioned earlier, a high absorption coefficient is not the single factor responsible for the LN-SSPD efficiency [20]. As fabricated samples have demonstrated, the fiber-to-waveguide coupling efficiency is relatively high for Ti:$LiNbO_3$ waveguides. Unfortunately, in our preliminary experiments we failed to reach the maximum internal detection efficiency of LN-SSPD. However, the last publication [18] demonstrated that this was possible. It should be noted that in [18] the LN-SSPD efficiency was tested at a much lower temperature (0.8 K) as compared with our experimental conditions which were the liquid-helium temperature at normal atmospheric pressure (4.2 K). Temperature lowering is one of the ways to increase the internal detection efficiency [26].

The other way is the optimization of the superconductive nanostructure through the adjustment of nanowire width and meander period [20], [27]–[29]. Moreover, according to the simulation results, variations in these parameters will not lead to a significant decrease in the maximum absorption coefficient.

VIII. Conclusion

To summarize, we have developed a new concept of a highly efficient integrated optical LN-SSPD. A hybrid waveguide structure consisting of a $LiNbO_3$ substrate with a conventional titanium in-diffused waveguide, NbN superconducting nanostructure and high-refractive-index dielectric stripe with a tapered waveguide mode transformer was proposed. TiO_2 and Si were considered as high-refractive-index materials. An optimal design of the hybrid waveguide structure and tapered waveguide mode transformer were theoretically analyzed. A high absorption coefficient was used as a criterion of the hybrid waveguide structure optimization. Si based structures give a higher light concentration and, hence, a higher absorption coefficient. However, they are very demanding to the technological accuracy. TiO_2 hybrid waveguide structures potentially can be produced by the standard thin-film deposition technique and contact photolithography. The estimated absorption coefficient $\alpha_{\mathrm{TiO2}} = 1.31\ \mathrm{dB}/\mu\mathrm{m}$ is four orders of magnitude higher than that for the SSPD with a standard titanium in-diffused waveguide, and a high transformation mode efficiency opens a way for fabrication of an integrated optical LN-SSPD with the efficiency comparable with other competing material platforms (Si, Si_3N_4 and A3B5 semiconductors).

References

[1] O. Alibart *et al.*, "Quantum photonics at telecom wavelengths based on lithium niobate waveguides," *J. Opt.*, vol. 18, Sep. 2016, Art. no. 104001.

[2] M. Bazzan and C. Sada, "Optical waveguides in lithium niobate: Recent developments and applications," *Appl. Phys. Rev.*, vol. 2 no. 4, Oct. 2015, Art. no. 040603.

[3] J. E. Toney, *Lithium Niobate Photonics.* Norwood, MA, USA: Artech House, 2015.

[4] A. Chen and E. J. Murphy, *Broadband Optical Modulators: Science, Technology, and Applications*. Boca Raton, FL, USA: CRC Press, 2012.

[5] E. L. Wooten *et al.*, "A review of lithium niobate modulators for fiber-optic communications systems," *IEEE J. Sel. Topics Quantum Electron.*, vol. 6, no. 69, pp. 69–82, Jan./Feb. 2000.

[6] Z. Zhu, S. Zhao, X. Li, K. Qu, and T. Lin, "A linearized analog photonic link based on a single z-Cut $LiNbO_3$ dual-output Mach–Zehnder modulator," *IEEE Photon. J.*, vol. 9, no. 3, Jun. 2017, Art. no. 7201810.

[7] C. S. Tsai, *Guided-Wave Acousto-Optics: Interactions, Devices, and Applications. Heidelberg*. Berlin, Germany: Springer, 1990.

[8] K. Buse, E. Krätzig, and K. H. Ringhofer, "Photorefractive materials: Properties and applications," *Appl. Phys. B.*, vol. 72, May 2001, Art. no. 633.

[9] D. Noriega Urquídez, S. Stepanov, H. Soto Ortiz, N. Toguzov, I. Ilichev, and A. Shamray, "Electrically controlled slow/fast propagation of 12.5-GHz light pulses in lithium niobate waveguide Bragg grating," *Appl. Phys. B.*, vol. 106, no. 1, pp. 51–56, Jan. 2012.

[10] M. Parfenov, A. Tronev, I. Ilichev, P. Agruzov, and A. Shamrai, "Precise correction of integrated optical power splitters based on lithium niobate substrates by photorefractive effect local excitation," *Appl. Phys. B.*, vol. 126, no. 5, Apr. 2020, Art. no. 93.

[11] G. N. Gol'tsman *et al.*, "Picosecond superconducting single-photon optical detector," *Appl. Phys. Lett.*, vol. 79, no. 6, pp. 705–707, Aug. 2001.

[12] S. Ferrari, C. Schuck, and W. Pernice, "Waveguide-integrated superconducting nanowire single-photon detectors," *Nanophotonics*, vol. 7, no. 11, pp. 1725–1758, Sep. 2018.

[13] P. Agruzov *et al.*, "Superconducting single-photon detector for lithium niobate integrated quantum photonic at telecom wavelengths," in *Proc. Conf. Lasers Electro-Opt. Europe Eur. Quantum Electron. Conf.*, Munich, Germany, 2019.

[14] M. G. Tanner *et al.*, "A superconducting nanowire single photon detector on lithium niobate," *Nanotechnology*, vol. 23, no. 50, Nov. 2012, Art. no. 505201.

[15] J. P. Höpker *et al.*, "Integrated transition edge sensors on titanium in-diffused lithium niobate waveguides," *APL Photon.*, vol. 4, May 2019, Art. no. 056103.

[16] J. P. Höpker *et al.*, "Integrated superconducting detectors on titanium in-diffused lithium niobate waveguides," in *Proc. OSA Tech. Dig. (Opt. Soc. Amer.)*, WA, DC, USA, 2020, Art. no. FF3D.6.

[17] A. Al Sayem, R. Cheng, S. Wang, and H. X. Tang, "Lithium-niobate-on-insulator waveguide-integrated superconducting nanowire single-photon detectors," *Appl. Phys. Lett.*, vol. 116, Apr. 2020, Art. no. 151102.

[18] J. P. Höpker *et al.*, "Integrated superconducting nanowire single-photon detectors on titanium in-diffused lithium niobate waveguides," *J. Phys.: Photon.*, vol. 3, no. 3, Jul. 2021, Art. no. 034022.

[19] A. M. Ionov *et al.*, "NbN films on vicinal to the X-cut of $LiNbO_3$ surfaces," *Mater. Lett.*, vol. 260, Nov. 2020, Art. no. 126918.

[20] O. Kahl, S. Ferrari, V. Kovalyuk, G. N. Goltsman, A. Korneev, and W. H. P. Pernice, "Waveguide integrated superconducting single-photon detectors with high internal quantum efficiency at telecom wavelengths," *Sci. Rep.*, vol. 5, Jun. 2015, Art. no. 10941.

[21] Y. Jia, L. Wang, and F. Chen, "Ion-cut lithium niobate on insulator technology: Recent advances and perspectives," *Appl. Phys. Rev.*, vol. 8, Feb. 2021, Art. no. 011307.

[22] M. Parfenov, P. Agruzov, I. Ilichev, and A. Shamray, "Simulation of Ti-indiffused lithium niobate waveguides and analysis of their mode structure," *J. Phys.: Conf. Ser.*, vol. 741, no. 1, Aug. 2016, Art. no. 012141.

[23] N. Mekada, M. Seino, Y. Kubota, and H. Nakajima, "Practical method of waveguide-to-fiber connection: Direct preparation of waveguide endface by cutting machine and reinforcement using ruby beads," *Appl. Opt.*, vol. 29, no. 34, pp. 5096–5102, Dec. 1990.

[24] M. Parfenov and A. Shamrai, "Improving the efficiency of the integrated optical superconducting single photon detector on a lithium niobate substrate by means of an additional cover layer with a high refractive index," *Tech. Phys. Lett.*, vol. 46, no. 8, pp. 819–822, Aug. 2020.

[25] R. Regener and W. Sohler, "Loss in low-finesse ti:Linbo3 optical waveguide resonators," *Appl. Phys. B.*, vol. 36, pp. 143–147, Mar. 1985.

[26] A. Korneev *et al.*, "Sensitivity and gigahertz counting performance of NbN superconducting single-photon detectors," *Appl. Phys. Lett.*, vol. 84, pp. 5338–5340, Jun. 2004.

[27] M. Hofherr *et al.*, "Intrinsic detection efficiency of superconducting nanowire single-photon detectors with different thicknesses," *J. Appl. Phys.*, vol. 108, Jul. 2010, Art. no. 014507.

[28] D. F. Marsili *et al.*, "Single-photon detectors based on ultranarrow superconducting nanowires," *Nano Lett.,* vol. 11, pp. 2048–2053, Apr. 2011.

[29] S. Miki *et al.*, "Large sensitive-area NbN nanowire superconducting single-photon detectors fabricated on single-crystal MgO substrates," *Appl. Phys. Lett.*, vol. 92, Feb. 2008, Art. no. 061116.

[30] T. Jin, J. Zhou, and P. T. Lin, "Mid-infrared electro-optical modulation using monolithically integrated titanium dioxide on lithium niobate optical waveguides," *Sci. Rep.*, vol. 9, Oct. 2019, Art. no. 15130.

[31] Y. Wang, Z. Chen, L. Cai, Y. Jiang, H. Zhu, and H. Hu, "Amorphous silicon-lithium niobate thin film strip-loaded waveguides," *Opt. Mater. Exp.*, vol. 7, no. 11, pp. 4018–4028, Nov. 2017.

[32] L. Cao, A. Aboketaf, Z. Wang, and S. Preble, "Hybrid amorphous silicon (a-Si:H)–$LiNbO_3$ electro-optic modulator," *Opt. Commun.*, vol. 330, pp. 40–44, Nov. 2014.

[33] X. Hu, C. W. Holzwarth, D. Masciarelli, E. A. Dauler, and K. K. Berggren, "Efficiently coupling light to superconducting nanowire single-photon detectors," *IEEE Trans. Appl. Supercond.*, vol. 19, no. 3, pp. 336–340, Jun. 2009.

[34] X. Guan, H. Hu, L. K. Oxenløwe, and L. H. Frandsen, "Compact titanium dioxide waveguides with high nonlinearity at telecommunication wavelengths," *Opt. Exp.*, vol. 26, no. 2, pp. 1055–1063, Jan. 2018.

[35] H. H. Li, "Refractive index of silicon and germanium and its wavelength and temperature derivatives," *J. Phys. Chem. Ref. Data*, vol. 9, pp. 561–658, 1980.

[36] A. F. Milton and W. K. Burns, "Mode coupling in optical waveguide horns," *IEEE J. Quantum Electron*, vol. 13, no. 10, pp. 828–835, Oct. 1977.

[37] D. Dai, Y. Tang, and J. E. Bowers, "Mode conversion in tapered submicron silicon ridge optical waveguides," *Opt. Exp.*, vol. 20, no. 12, pp. 13425–13439, May 2012.

[38] P. K. Tien, R. J. Martin, and S. Riva-Sanseverino, "Novel metal-clad optical components and method of isolating high-index substrates for forming integrated optical circuits," *Appl. Phys. Lett.*, vol. 27, no. 4, pp. 251–254, Aug. 1975.